Computational and Theoretical Chemistry 977 (2011) 13–21

Contents lists available at SciVerse ScienceDirect

Computational and Theoretical Chemistry

journal homepage: www.elsevier.com/locate/comptc

Theoretical considerations of secondary organic aerosol formation from H-abstraction of *p*-xylene

Shu-Xian Hu [a,d], Jian-Guo Yu [b], Shao-Meng Li [c], Eddy Y. Zeng [a,*]

[a] State Key Laboratory of Organic Geochemistry, Guangzhou Institute of Geochemistry, Chinese Academy of Sciences, Guangzhou 510640, China
[b] College of Chemistry, Beijing Normal University, Beijing 100875, China
[c] Environment Canada, 4905 Dufferin Street, Toronto, Ontario, Canada M3H 5T4
[d] Graduate School of the Chinese Academy of Sciences, Beijing 100049, China

ARTICLE INFO

Article history:
Received 14 March 2011
Received in revised form 31 August 2011
Accepted 31 August 2011
Available online 5 September 2011

Keywords:
p-Xylene
Atmospheric reaction
Degradation pathway
Density functional theory
Free energy profile

ABSTRACT

Xylenes are important constituents of many liquid fuels, as well as precursors of secondary organic aerosols (SOAs). To examine the mechanisms for formation of SOAs in the atmosphere, the abstraction reaction of *p*-xylene with OH and the secondary degradation channels of its intermediates were first and extensively investigated with density functional theory at the B3LYP/6-31+G (d, p) level. The result indicates that H-abstraction from methyl groups is a barrier-less path while that from phenyl groups require a free energy barrier of approximately 2.8 kcal mol^{-1}. Upon formation of *p*-xylyl, further addition by O_2 readily occurs to form peroxy radical. Subsequently, possible degradation channels for the formation of main products (*p*-tolualdehyde and *p*-quinone methide) have been determined in presence of NO. The free energy profile constructed shows that the entire reaction process is exothermic. In addition, the dipole moment of *p*-tolualdehyde is higher than that of *p*-xylene, consistent with their relative hygroscopic values. This indicates that the degradation products of *p*-xylene can readily immerse into the SOA phase, while *p*-xylene may be subject to further atmospheric degradation to form non-volatile compounds.

1. Introduction

The formation of secondary organic aerosols (SOAs) in the atmosphere has attracted a large amount of research interests because of its important implications for cloud formation, climatic change, visibility, and human health [1–8]. Aromatic hydrocarbons such as benzene, toluene, ethylbenzene, and xylenes, important constituents of gasoline fuels, automobile exhausts and evaporative emissions, are a major class of air pollutants, typically accounting for 30–40% of the total amount of volatile organic compounds (VOCs) emitted into the urban atmosphere [9,10]. In the atmosphere, due to their high potential to react with reactive species such as hydroxyl (·OH), nitrate radical (NO_3), and ozone (O_3), oxidation of aromatic compounds to form nonvolatile and semi-volatile organic chemicals is the primary fate process in the atmosphere [11–13]. In daytime, the reaction of aromatic hydrocarbons with hydroxyl radicals is the major atmospheric loss process [14–16]. Several previous experimental [17–19] and theoretical [20–26] studies have unraveled the elementary reactions involved in aromatic oxidation.

Partially due to the complicacy of VOCs species, therefore the compositions of SOA formed from VOCs, and the difficulty in direct measurements of the highly reactive intermediates during the oxidation reaction [27,28], experimental ratification of the entire reaction course has not yet obtained [1,3,10,29,30]. Previous studies showed that in the presence of OH radical the main reaction path is OH addition to the aromatic ring to form a xylene–OH adduct (consuming ~90% of OH radicals) with H-abstraction from one methyl group to form a methylbenzyl radical (consuming ~10% of OH radicals) being the minor route [18,31–34]. In addition, theoretical investigations have mainly focused on OH-addition to xylene and the fate of xylene–OH adducts and intermediates [15,26,31,34–36], whereas the H-abstraction mechanism for *p*-xylene oxidation following the initial OH attack and subsequent products have only been studied experimentally [22,25,37,38].

To fill the above-mentioned knowledge gap, a comprehensive theoretical investigation was undertaken to examine the mechanism for OH-initiated degradation of *p*-xylene and identify the dominant reaction pathways. Energy barriers and reaction energies for the formation of transition states and intermediates were obtained to determine the isomeric branching ratios of the degradation pathways. The objectives of the present study were to predict abstraction products from the OH and *p*-xylene reaction system

* Corresponding author. Tel.: +86 20 85291421; fax: +86 20 85290706.
E-mail address: eddyzeng@gig.ac.cn (E.Y. Zeng).

2210-271X/$ - see front matter © 2011 Elsevier B.V. All rights reserved.
doi:10.1016/j.comptc.2011.08.032

and to examine the mechanisms for atmospheric reaction of aromatic hydrocarbons with hydroxide radicals.

2. Computational details

Computations were performed using the GAUSSIAN 03 software package [39]. All radicals and molecules were calculated with density functional theory (DFT) and the optimized geometry data are presented in Tables S1–S35 of the Supplementary data. For the reactions, geometry optimization was executed using Becke's three-parameter hybrid method employing the LYP correlation functional (B3LYP) in conjunction with the split valence polarized and containing diffuse functions basis sets 6-31+G (d, p). Based on these optimized geometries, more accurate energies were obtained by performing single-point calculations using the 6-311+G (2d, 2p) basis sets for all elements. Frequency calculations were performed at the same level of theory as that used for geometry optimization on all stationary points of the reaction path to determine the nature of the stationary points and to obtain zero-point vibrational energy corrections (ZPE). The energies reported herein were corrected for zero-point vibrational effects. At the B3LYP/6-31+G (d, p) level of theory, we performed additional calculations using the intrinsic reaction coordinate (IRC) method, confirming each transition state uniquely connected with the reactant and product under investigation. For the calculation of total relative energy, the values of enthalpy, Gibbs free energy, and potential energy of triplet O_2 were used.

3. Results and discussion

3.1. Hydrogen abstraction

OH-initiated H-abstraction occurs potentially at two positions, i.e. methyl hydrogen and phenyl hydrogen. Starting from *p*-xylene, a pre-reactive [OH···xylene] complex is identified as a stable point (Figs. 1 and 2). Starting from pre-reactive complex, H-atom abstraction from one methyl (e.g. C_7 in Fig. 2), which is a barrierless path (about 1 kcal mol^{-1} in activation energy from experimental measurements [40]), can occur spontaneously. For the second path starting from pre-reactive complex, the geometries of the intermediate radical and its corresponding transition structure (TS1; Fig. 2) were optimized. The TS1 is characterized by an imaginary frequency of 1117*i* cm^{-1}, and its free energy barrier is approximately 2.8 kcal mol^{-1} (Table 1 and Fig. 7). The resulted products (IM1 and IM2), i.e. *p*-xylyl and di-*p*-tolyl radicals, lie at 27.6 and 5.2 kcal mol^{-1} lower than their corresponding reactants for both channels (Table 1 and Figs. 1 and 7). Therefore, H-atom abstraction from phenyl hydrogen to produce di-*p*-tolyl radical is more difficult than that from methyl hydrogen to yield *p*-xylyl.

At the TS1 (Fig. 2), the critical H_1—O distance is 1.27 Å, vastly different from 2.38 Å in pre-reactive complex. The abstracted hydrogen atom is actually leaving C_2 with the distance changing from 1.08 Å to 1.24 Å. The bonding of O, H_1 and C_2 almost lies in a straight line with an angle of 168.7°, which is increased from 74.5° in the pre-reactive complex. Downhill from TS1, H_1 is transferred from C_2 to O in OH radical to form a departing H_2O with a H_1—O bond length of 0.97 Å.

Abstraction of hydrogen from *p*-xylene leads to a shortened C—C bond linked to the site of abstraction. For *p*-xylyl radical (IM1; Fig. 2), the C—C bond length is decreased by 0.10 Å between C_1 and C_7 (methyl carbon). Similar C—C bond shortening is also observed for di-*p*-tolyl radical (IM2), i.e. the bond length is shortened by 0.03 Å between C_2—C_1 and C_2—C_3.

3.2. Hydrocarbonyl radicals

Under simulated atmospheric conditions in laboratory experiments, oxygen was reported to rapidly add to the alkyl radical (·R), forming primary peroxyl radical (·RO_2) [12,14]. The present study confirms that oxygen addition to the intermediates (IM1 and IM2) to form *p*-xylyl-O_2 radical (IM3) and di-*p*-tolyl peroxyl radical (IM4), respectively, is energy-barrier-free. These results are consistent with those in the literature [41,42]. Our calculations indicate that these two resulted products are 5.8 and 30.9 kcal mol^{-1} in free energy more stable than their corresponding reactants (IM1 and IM2) (Table 1 and Fig. 6). O_1 is attaching to reactive sites with the lengths of 1.48 Å for C_7—O_1 in IM3 and 1.41 Å for C_2—O_1 in IM4 (Fig. 2). No obvious bond length increases in C_3—H_3 and C_7—H_6 occur in IM3 and IM4. For IM3, the C_1—C_7 bond length is prolonged by 0.09 Å compared to that of IM1 (Fig. 2), because O which has a strong electron-withdrawing tendency could reduce electron density between C_1—C_7 (slightly less occupancy: 0.987 vs. 0.993 in the bond$_{C1-C7}$ for IM3 and IM1) For IM4, the C—C bond length next to the site of O_1 addition is increased by 0.02 Å relative to that of IM2 (Fig. 2), as the electron density in the π orbital above benzene ring is partially transferred to the newly formed C—O bond. Compared with the length of O═O bond in an oxygen molecule optimized with B3LYP, $^3O_2$-addition to the alkyl radicals results in an increase of the O—O bond from 1.22 to 1.33 Å.

3.3. Peroxyl radicals

Reactive peroxyl radicals have been found to degrade via three channels, i.e., IM3/IM4 + HO_2 → ROOH + $^3O_2$, IM3/IM4 + NO → RO + NO_2 and IM3/IM4 + NO → $RONO_2$ (Fig. 1) [3]. For the first channel, the reactions of IM3/IM4 with HO_2 to form hydroxperoxides, i.e. *p*-methylphenyl hydroperoxide (P1) and 2,5-dimethyl phenyl hydroperoxide (P2) (Fig. 3), are exothermic by 32.1 and 31.9 kcal mol^{-1}, respectively (Table 2 and Figs. 8 and 9). These results are consistent with those from previous experimental studies [3,8].

Also consistent with previous experimental results [3,29], the reaction of IM3 with nitrogen oxide under the presence of NO is predicted to occur via two pathways by our calculations. One pathway is unimolecular decomposition via TS2 involving O_1—O_2 cleavage. Another is an isomeric process with *p*-xylyl nitrate formation (P3) that has a free energy barrier of 30.1 kcal mol^{-1} (Table 2 and Figs. 4 and 8). The structures of peroxyl radical–NO complex (IM7), TS2 which was confirmed by an imaginary frequency of 526*i* cm^{-1}, IM8, and the resulted radical intermediate, *p*-xylyl-O radical (IM9), are also obtained (Fig. 4). The free energy barrier with zero-point correction of reaction of IM3 with NO is 29.2 kcal mol^{-1} (Table 2 and Fig. 8). This barrier is consistent with the results for atmospheric photooxidation of methyl vinyl ether [43]. It is noted that at TS2 (Fig. 4) the nascent N—O_2 bond is 1.48 Å, which is decreased from 3.02 Å in IM7, and the O_1—O_2 bond is elongated from 1.32 Å to 1.44 Å. At IM8 (Fig. 4), this distance is further elongated to 3.23 Å, while the N—O_2 distance is shortened to 1.20 Å. The interaction between C_7 and O_1 therefore has become strengthened, as its bond distance is shortened from 1.48 Å at IM7 to 1.45 Å at TS2 and to 1.36 Å at IM9, which thereby lowers the energy of the resulted radical. As mentioned above, the other process involving the formation of *p*-xylyl nitrate (P3) is exothermic by 41.3 kcal mol^{-1} (Table 2 and Fig. 8), and its transition structure (TS3) is characterized by an imaginary frequency of 251*i* cm^{-1}. At TS3 (Fig. 4), the distance of O_1—N closure is 1.47 Å, sharply decreased from 2.90 Å at IM8, and the O_1—C_7 and N—O_2 bonds are elongated from 1.36 and 1.20 Å to 1.46 and 1.34 Å, respectively. At P3 (Fig. 4), the O_1—C_7, N—O_2 and newly formed O_1—N bonds are 1.47, 1.21 and 1.41 Å, respectively, and other geometrical parameters are close to those in IM8.

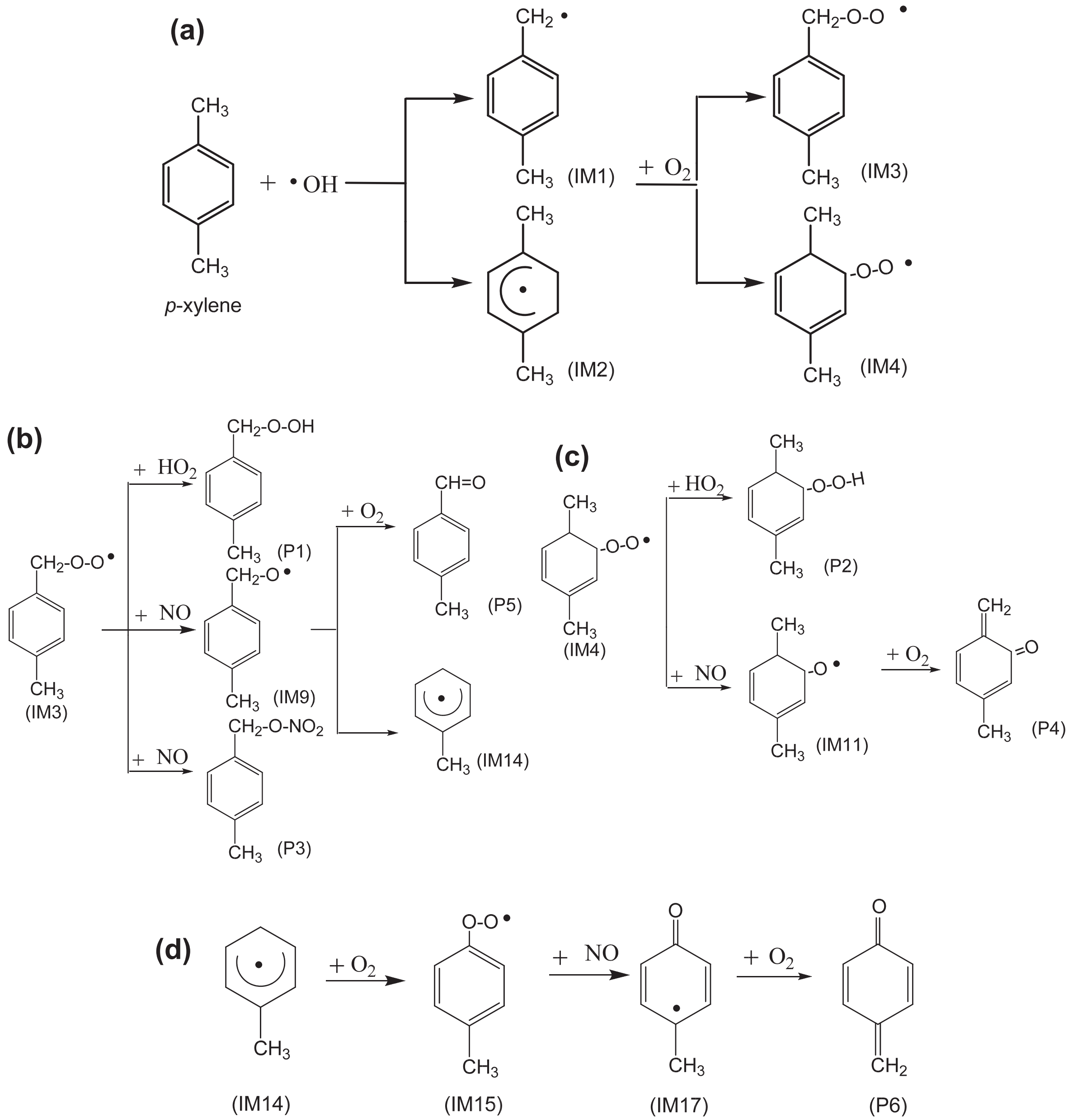

Fig. 1. (a) Proposed pathways for the reactions of *p*-xylene with OH radical and molecular oxygen; (b) proposed pathways for the reaction of *p*-xylyl peroxy radical in the present of O_2/NO; (c) proposed pathways for the reaction of di-*p*-tolyl peroxy radical in the presence of O_2/NO; (d) proposed pathways for the reactions of p-tolyl radical in the presence of O_2/NO.

Unimolecular decomposition, with a lower energy barrier than that with the isomeric process, is feasible (Table 2 and Fig. 8) and probably significant in the atmosphere where NO is abundant. Atkinson [12] observed experimentally that the formation yields of organic nitrates declined with increasing temperature and decreasing pressure. On the other hand, how significant the yield of P3 is dependent on temperature and pressure needs further molecular dynamics simulation, which has not been done in the present study.

For the reaction of IM4 with NO, a IM14–NO complex (IM10) is formed and subsequent O_1–O_2 bond scission leads to the formation of IM11 and NO_2, which is exothermic by 46.4 kcalmol^{-1} via a free energy barrier of 26.4 kcal mol^{-1} (Table 2 and Fig. 9). Its transition structure (TS4) is characterized by an imaginary frequency of 673*i* cm^{-1}. In TS4 (Fig. 4), the critical N—O_2 distance is 1.54 Å, dramatically decreased from 2.98 Å in IM10, and the O_1—O_2 distance is increased from 1.33 to 1.46 Å. Downhill from TS4, O_2 is approaching N in NO to produce NO_2 and IM15, in which the C—O_1 bond length is reduced to 1.26 Å.

3.4. Alkoxy radicals

The formation of 2,4-cyclohexadien-1-one (P4), the only plausible destiny of 2,5-xylyloxy radical (IM11) in the atmosphere, is resulted from reaction of IM11 with $^3O_2$ via TS5 with a free energy barrier of 26.1 kcal mol^{-1} (Table 2 and Fig. 9). The H-atom transfer scenario leads to an increase of the C_7—H_1 bond from 1.10 Å in the complex (IM12) to 1.35 Å in TS5 and a decrease of the C_1—C_7 bond from 1.50 Å to 1.40 Å. The formation of P4, in which the C_1—C_7 bond is stretched by 0.5 Å from TS5, leads to 15.4 kcal mol^{-1} more energetically unfavorable than IM11 (Figs. 5 and 9).

For IM9, a reactive radical, two primary degradation reactions are possible: IM9 + $^3O_2$ → P5 (*p*-tolualdehyde) + HO_2 and IM9 → IM14 (*p*-tolyl radical) + CH_2O (Fig. 1). The reaction of

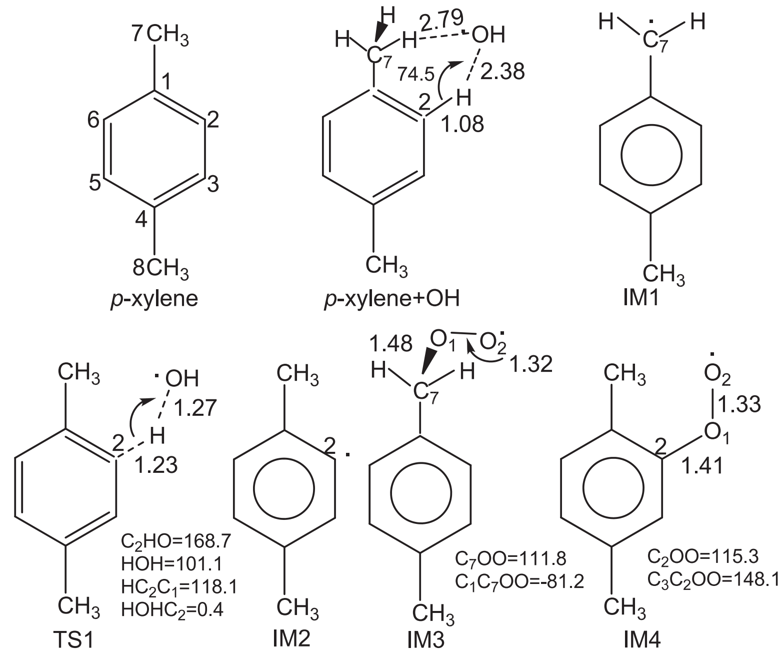

Fig. 2. Optimized geometries of the reactant, intermediates, transition structures and products for H-abstraction reaction of *p*-xylene and OH radical in the presence of O_2 at the B3LYP/6-31+G (d, p) level of theory.

Table 1
Relative enthalpy (ΔH^0), relative gibbs free energy (ΔG^0), relative potential energy (ΔE^0), activation potential energy ($\Delta E^{\pm}$), activation gibbs free energy ($\Delta G^{\pm}$) and branching ratio for the reaction of *p*-xylene with OH radical at 298 K.

Reaction[a]	TS	$\Delta G^{\pm b}$	$\Delta E^{\pm b}$	ΔH^{0b}	ΔG^{0b}	ΔE^{0b}
p-Xylene + OH → complex		–	–	−3.8 −2.35/−2.26/2.03[c]	5.1	−3.5
Complex → IM1 + H_2O	–	–	 −1.38/−2.08[d]	−24.2 −22.94[c]	−32.7	−24.4 −6.84/−12.54[d]
Complex → IM2 + H_2O	TS1	2.8	3.1 9.08[e]	−0.8 −13.88[c]	−10.3	−1.3 −0.21[e]

[a] IM and TS represent intermediate product and transition state, respectively.
[b] Unit in kcal mol^{-1}.
[c] Calculated values using B3LYP/6-31G* method by Sun et al. [43].
[d] Calculated values using B3LYP/6-31G (d.p) method by Huang et al.[46].
[e] Calculated values using BHandHLYP/6-311++G** method by Uc et al. [40].

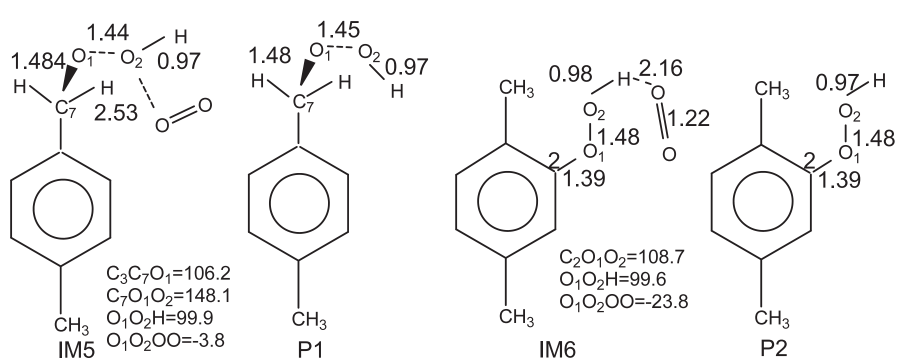

Fig. 3. Optimized geometries of the reactant, intermediates, transition structures and products involved in the reaction of IM3 with HO_2 at the B3LYP/6-31+G (d, p) level of theory.

p-xylyl-O radical with $^3O_2$ has been predicted to be a significant degradation pathway in experimental studies [12,33], and is corroborated in the present study with a feasible free energy barrier height of 8.0 kcal mol^{-1} (Table 2 and Fig. 8). The corresponding transition structure (TS6) is characterized by an imaginary frequency of 1171*i* cm^{-1}, in which the distance for breaking the C_7—H_1 bond is 1.35 Å and the distance for O—H_1 closure is 1.50 Å (Fig. 5). In P5, which is 86.4 kcal mol^{-1} more stable than its corresponding precursors, the bond lengths of C_1—C_7 and C_2—O are 1.35 Å and 1.22 Å, respectively (Table 2 and Fig. 8). In the transition

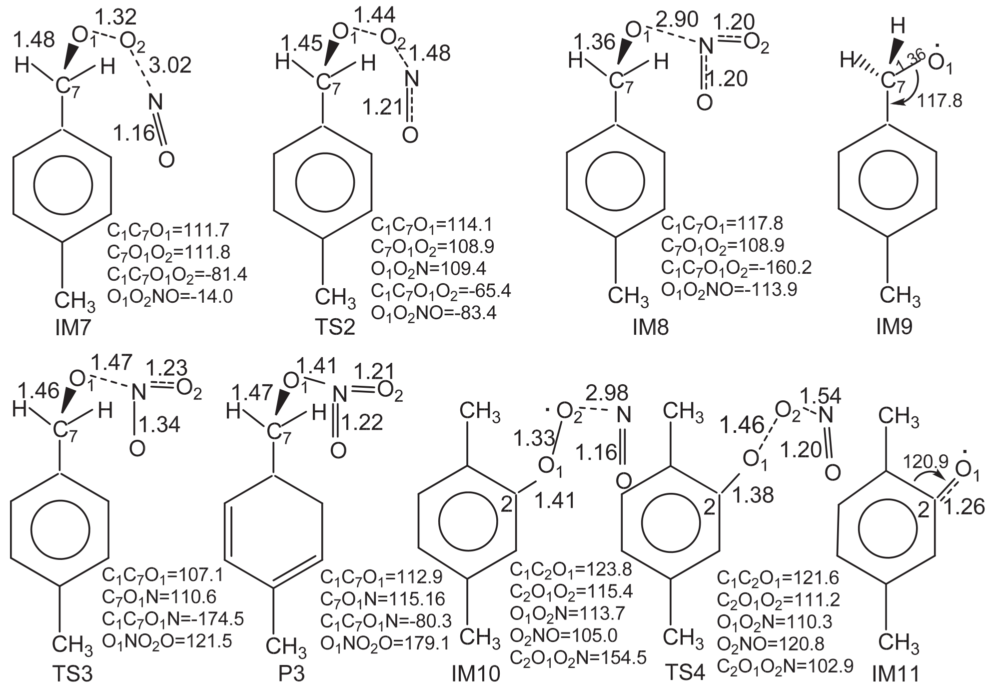

Fig. 4. Optimized geometries of the reactant, intermediates, transition structures and products involved in the reaction of IM3 and IM4with NO at the B3LYP/6-31+G (d, p) level of theory.

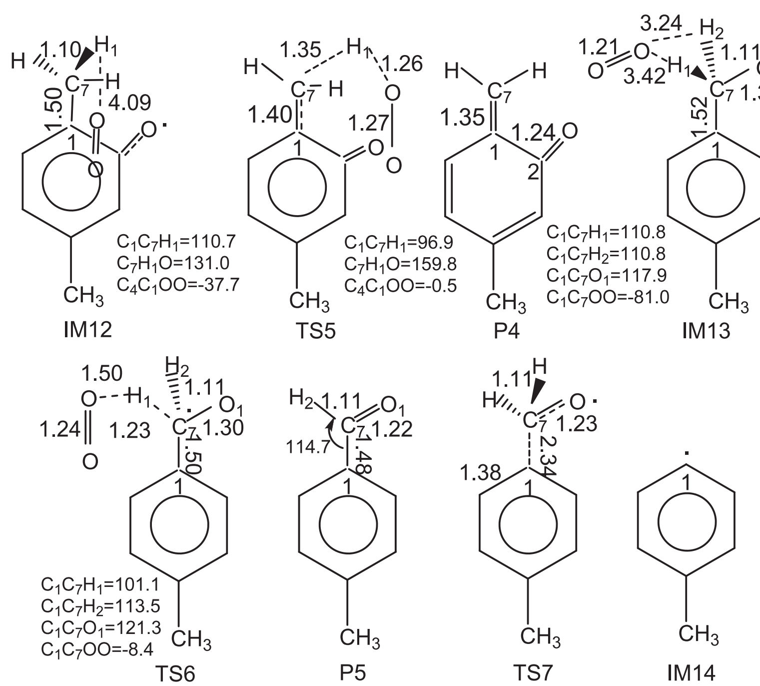

Fig. 5. Optimized geometries of the reactant, intermediates, transition structures and products involved in the reaction of IM3 and IM4 with O_2 at the B3LYP/6-31+G (d, p) level of theory.

structure of the unimolecular decomposition of IM9, i.e. TS7, which is characterized by an imaginary frequency of $144i$ cm^{-1}, the C_1—C_7 bond length is 2.34 Å, increased from 1.52 Å in IM9 and other geometrical parameters are close to those in IM9 (Fig. 5). With a free energy barrier of 23.8 kcal mol^{-1} (Table 2), this process is less likely to occur than the reaction of IM9 with $^3O_2$.

3.5. Reaction of p-tolyl radical with oxygen

In the troposphere, the reaction of *p*-tolyl radical (IM14) with oxygen is a degradation pathway, which is similar to that of IM2, via a barrier-free process to generate a new intermediate radical (IM15), which is 34.3 kcal mol^{-1} below IM14. This process is

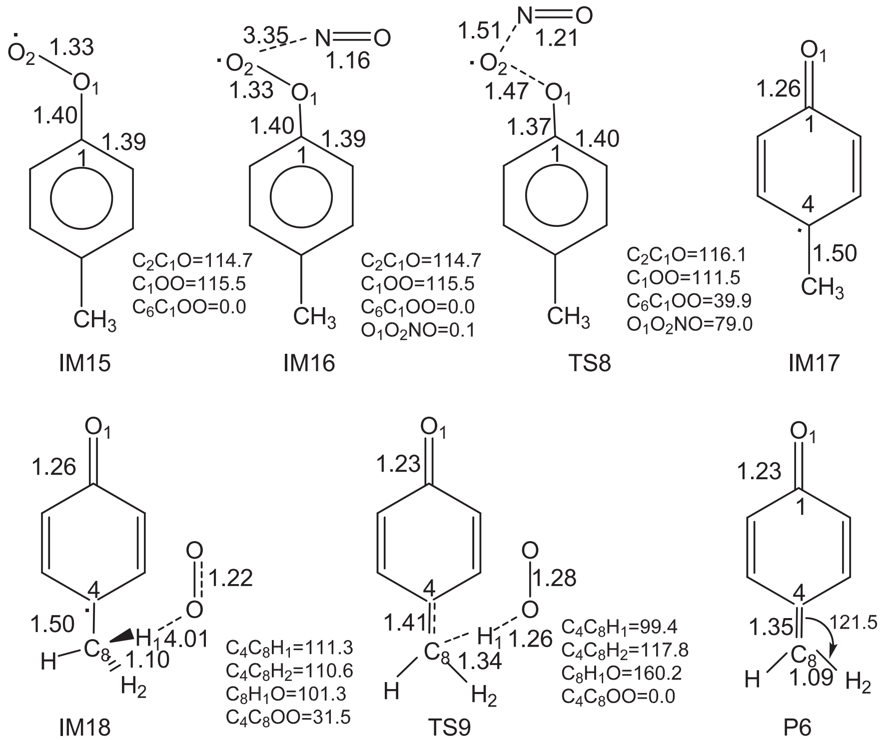

Fig. 6. Optimized geometries of the reactant, intermediates, transition structures and products involved in the reaction of IM14 with O_2/NO at the B3LYP/6-31+G (d, p) level of theory.

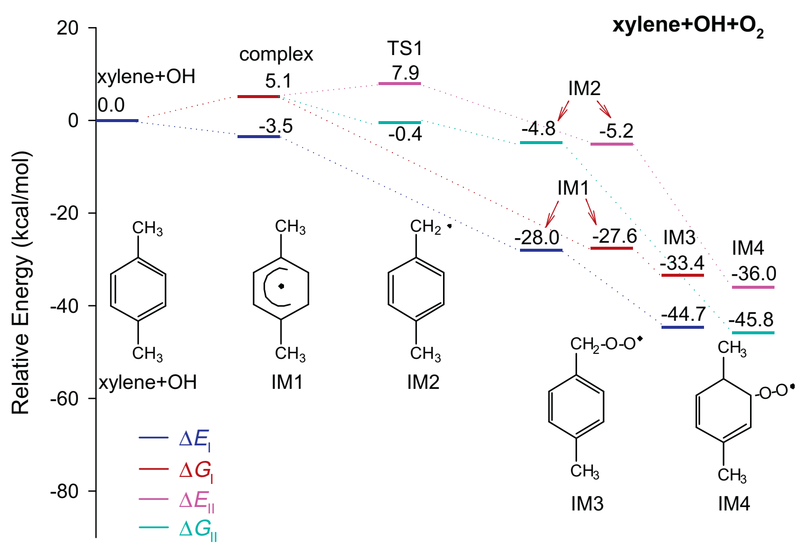

Fig. 7. Energy profile for the reaction of *p*-xylene with OH in the presence of O_2.

consistent in the foregoing results and literatures [41,42]. The newly formed C_1—O_1 bond is 1.40 Å in IM15, and the O_1—O_2 bond is 1.33 Å compared to 1.22 Å in oxygen. Subsequently, N atom in NO attacks O_2 in IM15 to form IM 17 and a molecular NO_2 with a transition structure (TS8) involved, which is characterized by 648*i* cm^{-1}. This process is exothermic by 31.8 kcal mol^{-1} with a free energy barrier of 28.3 kcal mol^{-1}. In IM17, the C_1—O_1 bond length is reduced to 1.26 Å from 1.40 Å in IM15. In addition, the reaction of IM17 with oxygen generates alkenyl ketone (P6) that is similar to the carbonyl species produced by the IM11 + $^3O_2$ reaction and involves the migration of hydrogen in methyl group to another reactant, $^3O_2$, via IM18 and TS9 to form P6 and a molecular HO_2. In TS9, which is characterized by an imaginary frequency of 1467*i* cm^{-1} and is –80.0 kcal mol^{-1} on the free-energy curve, the distance of C_8—H_1 is lengthened to 1.34 Å from 1.10 Å in IM18 and the C_4—C_8 bond is reduced by 0.09 Å from 1.50 Å. The formation of *p*-quinone methide (P6), in which the C_4—C_8 and C_1—O_1 bond lengths are 1.35 and 1.23 Å, respectively, is exothermic by 25.0 kcal mol^{-1} (Table 2 and Figs. 6 and 10).

It can be deduced from the results presented above that methyl-H-abstraction and further degradation reaction are the dominant pathways and the formation of *p*-xylyl-O radical is the rate-determining step for reaction of *p*-xylene in the atmosphere. In addition, the total free energy is lowered for the processes to

Table 2
Relative enthalpy (ΔH^0), relative Gibbs free energy (ΔG^0), and relative potential energy (ΔE^0) for all paths, activation potential energy ($\Delta E^{\pm}$), and activation Gibbs free energy (ΔG°) at 298 K calculated for secondary reactions in the presence of O_2/NO.

Reaction[a]	TS	$\Delta G^{\pm}$ [b]	$\Delta E^{\pm}$ [b]	ΔH^0 [b]	ΔG^0 [b]	ΔE^0 [b]
IM1 + $^3O_2$ → IM3	–	–	–	−18.0	−5.8	−16.7
	–	–	–	−15.4[c]		
IM2 + $^3O_2$ → IM4	–	–	–	−41.9	−30.9	−41.0
	–	–	–			−42.4[d]
IM3 + HO_2 → IM5	–	–	–	5.1	13.5	4.4
IM5 → P1 + O_2	–	–	–	−31.3	−32.1	−31.9
IM4 + HO_2 → IM6	–	–	–	4.4	11.6	3.9
IM6 → P2 + O_2	–	–	–	−33.3	−31.9	−33.4
IM3 + NO → IM7	–	–	–	0.2	4.4	−0.5
IM7 → IM9 + NO_2	TS2	29.2	25.7	−16.1	−21.2	−15.2
			29.30[e]	−15.28[e]		
IM7 → P3	TS3	36.8	32.7	−49.2	−41.3	−47.3
IM4 + NO → IM10				0.2	5.2	−0.3
IM10 → IM11 + NO_2	TS4	26.4	22.6	−41.0	−46.4	−40.1
IM11 + $^3O_2$ → IM12				0.6	4.5	−0.1
IM12 → P4 + HO_2	TS5	26.1	20.1	14.9	15.4	15.7
IM9 + $^3O_2$ → IM13				−0.4	5.6	−0.1
IM13 → P5 + HO_2	TS6	8.0	4.4	−81.4	−86.4	−81.5
IM9 → IM14 + CH_2O	TS7	23.8	25.0	24.8	13.4	24.1
IM14 + $^3O_2$ → IM15	–	–	–	−45.4	−34.3	−44.6
IM15 + NO → IM16				−0.6	6.1	−0.1
IM16 → IM17 + NO_2	TS8	28.3	24.9	−37.1	−44.1	−36.3
IM17 + $^3O_2$ → IM18				0.7	4.0	−0.1
IM18 → P6 + HO_2	TS9	26.7	18.9	12.2	−25.0	−13.1

[a] IM and TS represent intermediate product and transition state, respectively.
[b] Unit in kcal mol^{-1}.
[c] Calculated values using B3LYP/6-311G (2d, d, p) method by Murakami et al. [41] .
[d] Calculated values using B3LYP/6-311++G** method by Tokmakov et al. [47].
[e] Calculated values using B3LYP/6-31G* method by Sun et al. [43].

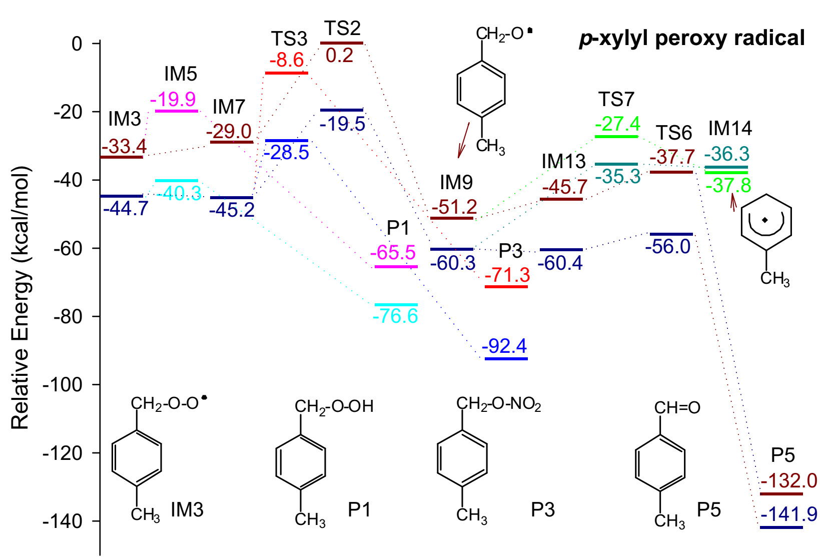

Fig. 8. Energy profile for the reaction pathways of IM3 in the presence of O_2/NO. Dark red: ΔG_{NO} and ΔG_{C-C}; pink: ΔG_{HO2}; green: ΔG_{O2}; dark blue: ΔE_{NO} and ΔE_{C-C}; cyan: ΔE_{HO2}; and dark cyan: ΔE_{O2}. (For interpretation of the references to colour in this figure legend, the reader is referred to the web version of this article.)

generate *p*-tolualdehyde (P5) and *p*-quinone methide (P6) compared to the initial reactants (*p*-xylene + OH radical) amount to 132.0 and 96.5 kcal mol^{-1}, respectively, in the presence of O_2/NO (Figs. 9 and 10).

3.6. Environmental significance

In the process of forming SOAs, the key quantity is hygroscopic property, involving the knowledge of molecular polarity with respect to water-solubility, hydration and nucleation, and adsorptivity of the molecule. The values of these parameters can predicted according to their dipole moments obtained from quantum chemical computation. A chemical with a larger dipole moment tend to more easily partition from the gaseous phase to the aqueous phase compared to a molecule with smaller dipole moment. Calculated dipole moments for *p*-xylene and corresponding products (P1, P2, P3, P4, P5 and P6) are 0.02, 2.98, 2.08, 4.98, 4.14, 4.24 and 4.93D, respectively. It is apparent that the polarities of the degradation products are remarkably larger than that of *p*-xylene, which is also consistent with their relative hygroscopic values (water solubilities

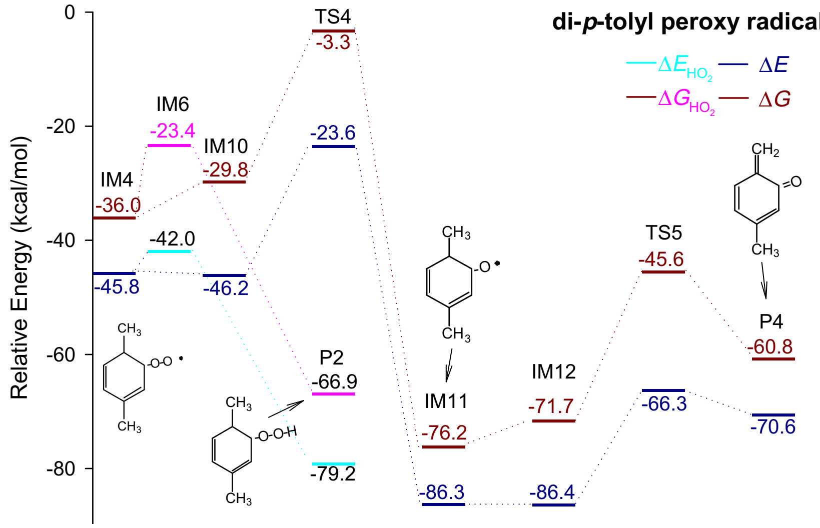

Fig. 9. Energy profile for the reaction pathways of IM4 in the presence of O_2/NO.

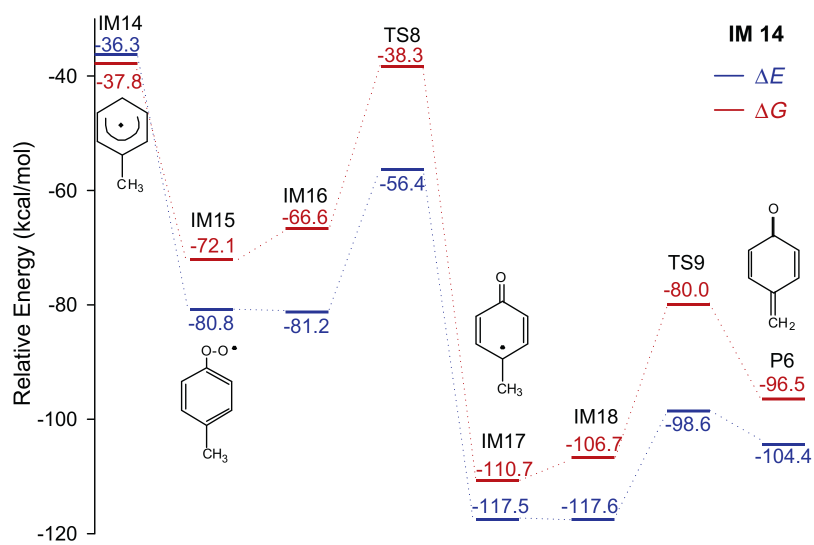

Fig. 10. Energy profile for the reaction pathways of IM14 in the presence of O_2/NO.

for *p*-xylene and *p*-tolualdehyde are 0.2 and 3 g/L, respectively) [44], and somewhat predict the massive contributions of *p*-xylene degradation products to the formation of SOAs. This result is consistent with a previous experimental result in which higher ratio of secondary VOC in SOAs in summer than in other seasons was observed [45].

4. Conclusions

The OH radical-initiated atmospheric degradation of *p*-xylene is predicted to occur favorably under the generally encountered atmospheric conditions. For H-abstraction from alkyls, the H atoms from $-CH_3$ portions are more active than those in $-C_6H_5$ groups. *p*-Xylyl nitrate, 2,4-cyclohexadien-1-one, *p*-tolualdehyde and *p*-quinone methide are generated from reaction of *p*-xylyl with O_2/NO. The formation of *p*-tolualdehyde is preferred over that of *p*-xylyl nitrate, and the formation of *p*-quinone methide involves further reactions of *p*-tolyl in the atmosphere. These reactions have excellent selectivity and differ considerably from other competitive reactions in terms of $\Delta G^{\pm}$ and ΔG^0. Moreover, the enhanced polarity and solubility of the degradation products from *p*-xylene may be the causes for their significant contributions to the formation of SOAs via nucleation, hydration and adsorption processes in the troposphere.

Acknowledgements

Financial support from the Earmarked Fund of the State Key Laboratory of Organic Geochemistry (SKLOG2009A04) and the National Natural Science Foundation of China (40821003 and 40928003) is greatly appreciated. This is contribution No. IS-1385 from GIGACS.

Appendix A. Supplementary material

Supplementary data associated with this article can be found, in the online version, at doi:10.1016/j.comptc.2011.08.032.

References

[1] M. Huang, W. Zhang, L. Hao, Z. Wang, W. Zhao, X. Gu, X. Guo, X. Liu, B. Long, L. Fang, Laser desorption/ionization mass spectrometric study of secondary organic aerosol formed from the photooxidation of aromatics, J. Atmos. Chem. 58 (2007) 237–252.

[2] Y. Nakashima, N. Kamei, S. Kobayashi, Y. Kajii, Total OH reactivity and VOC analyses for gasoline vehicular exhaust with a chassis dynamometer, Atmos. Environ. 44 (2010) 468–475.

[3] J.H. Kroll, J.H. Seinfeld, Chemistry of secondary organic aerosol: formation and evolution of low-volatility organics in the atmosphere, Atmos. Environ. 42 (2008) 3593–3624.

[4] J. Noda, R. Volkamer, M.J. Molina, Dealkylation of alkylbenzenes: a significant pathway in the toluene, *o*-, *m*-, *p*-xylene + OH reaction, J. Phys. Chem. A 113 (2009) 9658–9666.

[5] V.I. Baranov, L.A. Gribov, V.E. Dridger, M.K. Iskhakov, I.V. Mikhailov, A method for simulation of photochemical processes and calculation of quantum yields of reactions, Photochemistry 43 (2009) 416–423.

[6] R.M. Healy, B. Temime, K. Kuprovskyte, J.C. Wenger, Effect of relative humidity on gas/particle partitioning and aerosol mass yield in the photooxidation of *p*-xylene, Environ. Sci. Technol. 43 (2009) 1884–1889.

[7] A. Hachimi, T. Chafik, D. Bianchi, Adsorption models and heat of adsorption of adsorbed ortho di-methyl benzene species on silica by using temperature programmed adsorption equilibrium methods, Appl. Catal., A 335 (2008) 220–229.

[8] M. Camredon, B. Aumont, J. Lee-Taylor, S. Madronich, The SOA/VOC/NO_x system: an explicit model of secondary organic aerosol formation, Atmos. Chem. Phys. 7 (2007) 5599–5610.

[9] R. Volkamer, U. Platt, K. Wirtz, Primary and secondary glyoxal formation from aromatics: experimental evidence for the bicycloalkyl-radical pathway from benzene, toluene, and *p*-xylene, J. Phys. Chem. A 105 (2001) 7865–7874.

[10] H.L. Bethel, J. Arey, R. Atkinson, Products of the OH radical-initiated reaction of 3-hexene-2,5-dione, Environ. Sci. Technol. 35 (2001) 4477–4480.

[11] D. Zhang, R. Zhang, Mechanism of OH formation from ozonolysis of isoprene: a quantum-chemical study, J. Am. Chem. Soc. 124 (2002) 2692–2703.

[12] R. Atkinson, Atmospheric chemistry of VOCs and NO_x, Atmos. Environ. 34 (2000) 2063–2101.

[13] R. Atkinson, Rate constants for the atmospheric reactions of alkoxy radicals: an updated estimation method, Atmos. Environ. 41 (2007) 8468–8485.

[14] R. Atkinson, J. Arey, Atmospheric degradation of volatile organic compounds, Chem. Rev. 103 (2003) 4605–4638.

[15] V.H. Uc, J.R. Alvarez-Idaboy, A. Galano, A. Vivier-Bunge, Theoretical explanation of nonexponential OH decay in reactions with benzene and toluene under pseudo-first-order conditions, J. Phys. Chem. A 112 (2008) 7608–7615.

[16] R. Koch, R. Knispel, M. Elend, M. Siese, C. Zetzsch, Consecutive reactions of aromatic–OH adducts with NO, NO_2 and O_2: benzene, toluene, *m*- and *p*-xylene, hexamethylbenzene, phenol, m-cresol and aniline, Atmos. Chem. Phys. 6 (2006) 7623–7656.

[17] M. Jang, R.M. Kamens, Characterization of secondary aerosol from the photooxidation of toluene in the presence of NO_x and 1-propene, Environ. Sci. Technol. 35 (2001) 3626–3639.

[18] D.F. Smith, T.E. Kleindienst, C.D. McIver, Primary product distributions from the reaction of OH with m-, p-xylene, 1,2,4- and 1,3,5-trimethylbenzene, J. Atmos. Chem. 34 (1999) 339–364.

[19] H.J.L. Forstner, R.C. Flagan, J.H. Seinfeld, Secondary organic aerosol from the photooxidation of aromatic hydrocarbons: molecular composition, Environ. Sci. Technol. 31 (1997) 1345–1358.

[20] Y. Murakami, T. Oguchi, K. Hashimoto, Y. Nosaka, Density functional study of the high-temperature oxidation of *o*-, *m*- and *p*-xylyl radicals, J. Phys. Chem. A 113 (2009) 10652–10666.

[21] D.R. Glowacki, L. Wang, M.J. Pilling, Evidence of formation of bicyclic species in the early stages of atmospheric benzene oxidation, J. Phys. Chem. A 113 (2009) 5385–5396.

[22] G.d. Silva, M.R. Hamdan, J.W. Bozzelli, Oxidation of the benzyl radical: mechanism, thermochemistry, and kinetics for the reactions of benzyl hydroperoxide, J. Chem. Theory Comput. 5 (2009) 3185–3194.

[23] I. Suh, R. Zhang, L.T. Molina, M.J. Molina, Oxidation mechanism of aromatic peroxy and bicyclic radicals from OH–toluene reactions, J. Am. Chem. Soc. 125 (2003) 12655–12665.

[24] I. Suh, D. Zhang, R. Zhang, L.T. Molina, M.J. Molina, Theoretical study of OH addition reaction to toluene, Chem. Phys. Lett. 364 (2002) 454–462.

[25] G.d. Silva, C.-C. Chen, J.W. Bozzelli, Toluene combustion: reaction paths, thermochemical properties, and kinetic analysis for the methylphenyl radical + O_2 reaction, J. Phys. Chem. A 111 (2007) 8663–8676.

[26] J.M. Andino, J.N. Smith, R.C. Flagan, W.A. Goddard, J.H. Seinfeld, Mechanism of atmospheric photooxidation of aromatics: a theoretical study, J. Phys. Chem. 100 (1996) 10967–10980.

[27] E.G. Alvarez, J. Viidanoja, A. Muñoz, K. Wirtz, J. Hjorth, Experimental confirmation of the dicarbonyl route in the photo-oxidation of toluene and benzene, Environ. Sci. Technol. 41 (2007) 8362–8369.

[28] M.J. Molina, R. Zhang, K. Broekhuizen, W. Lei, R. Navarro, L.T. Molina, Experimental study of intermediates from OH-initiated reactions of toluene, J. Am. Chem. Soc. 121 (1999) 10225–10226.

[29] H.L. Bethel, R. Atkinson, J. Arey, Products of the gas-phase reactions of OH radicals with p-xylene and 1,2,3- and 1,2,4-trimethylbenzene: effect of NO_2 concentration, J. Phys. Chem. A 104 (2000) 8922–8929.

[30] M.-Q. Huang, W.-J. Zhang, L.-Q. Hao, Z.-Y. Wang, W.-W. Zhao, X.-J. Gu, L. Fang, Low-molecular weight and oligomeric components in secondary organic aerosol from the photooxidation of *p*-xylene, J. Chin. Chem. Soc. 55 (2008) 456–463.

[31] S. Olivella, A. Solé, J.M. Bofill, Theoretical mechanistic study of the oxidative degradation of benzene in the troposphere: reaction of benzene–HO radical adduct with O_2, J. Chem. Theory Comput. 5 (2009) 1607–1623.

[32] R. Atkinson, S.M. Aschmann, J. Arey, Formation of ring-retaining products from the OH radical-initated reactions of *o*-, *m*-, and *p*-xylene, Int. J. Chem. Kinet. 23 (1991) 77–97.

[33] J. Zhao, R. Zhang, K. Misawa, K. Shibuya, Experimental product study of the OH-initiated oxidation of *m*-xylene, J. Photochem. Photobiol. A: Chemistry 176 (2005) 199–207.

[34] T.H. Lay, J.W. Bozzelli, Atmospheric photochemical oxidation of benzene: benzene + OH and the benzene–OH adduct (hydroxyl-2,4-cyclohexadienyl) + O_2, J. Phys. Chem. 100 (1996) 6543–6554.

[35] J. Fan, R. Zhang, Atmospheric oxidation mechanism of *p*-xylene: a density functional theory study, J. Phys. Chem. A 110 (2006) 7728–7737.

[36] J. Fan, R. Zhang, Density functional theory study on OH-initiated atmospheric oxidation of *m*-xylene, J. Phys. Chem. A 112 (2008) 4314–4323.

[37] R. Atkinson, J. Arey, Atmospheric chemistry of gas-phase polycyclic aromatic hydrocarbons: formation of atmospheric mutagens, Environ. Health Perspect. 104 (1994) 117–126.

[38] F.A. Villamena, J.K. Merle, C.M. Hadad, J.L. Zweier, Rate constants of hydroperoxyl radical addition to cyclic nitrones: a DFT study, J. Phys. Chem. A 111 (2007) 9995–10001.

[39] M.J. Frisch, G.W. Trucks, H.B. Schlegel, G.E. Scuseria, M.A. Robb, J.R. Cheeseman, J.A. Montgomery Jr., T. Vreven, K.N. Kudin, J.C. Burant, J.M. Millam, S.S. Iyengar, J. Tomasi, V. Barone, B. Mennucci, M. Cossi, G. Scalmani, N. Rega, G.A. Petersson, H. Nakatsuji, M. Hada, M. Ehara, K. Toyota, R. Fukuda, J. Hasegawa, M. Ishida, T. Nakajima, Y. Honda, O. Kitao, H. Nakai, M. Klene, X. Li, J.E. Knox, H.P. Hratchian, J.B. Cross, C. Adamo, J. Jaramillo, R. Gomperts, R.E. Stratmann, O. Yazyev, A.J. Austin, R. Cammi, C. Pomelli, J.W. Ochterski, P.Y. Ayala, K. Morokuma, G.A. Voth, P. Salvador, J.J. Dannenberg, V.G. Zakrzewski, S. Dapprich, A.D. Daniels, M.C. Strain, O. Farkas, D.K. Malick, A.D. Rabuck, K. Raghavachari, J.B. Foresman, J.V. Ortiz, Q. Cui, A.G. Baboul, S. Clifford, J. Cioslowski, B.B. Stefanov, G. Liu, A. Liashenko, P. Piskorz, I. Komaromi, R.L. Martin, D.J. Fox, T. Keith, M.A. Al-Laham, C.Y. Peng, A. Nanayakkara, M. Challacombe, P.M.W. Gill, B. Johnson, W. Chen, M.W. Wong, C. Gonzalez, J.A. Pople, in: Gaussian, Inc., Pittsburgh, 2004.

[40] V.H. Uc, J.R. Alvarez-Idaboy, A. Galano, I. García-Cruz, A. Vivier-Bunge, Theoretical determination of the rate constant for OH hydrogen abstraction from toluene, J. Phys. Chem. A 110 (2006) 10155–10162.

[41] Y. Murakami, T. Oguchi, K. Hashimoto, Y. Nosaka, Theoretical study of the benzyl + O_2 reaction: kinetics, mechanism, and product branching ratios, J. Phys. Chem. A 111 (2007) 13200–13208.

[42] G. da Silva, J.W. Bozzelli, Variational analysis of the phenyl + O_2 and phenoxy + O reactions, J. Phys. Chem. A 112 (2008) 3566–3575.

[43] X. Sun, M. He, Q. Zhang, W. Wang, A.F. Jalbout, Quantum chemical study on the atmospheric photooxidation of methyl vinyl ether (MVE), J. Mol. Struct. 868 (2008) 87–93.

[44] D. Mackay, W.Y. Shiu, K.-C. Ma, S.C. Lee, Handbook of physical–chemical properties and environmental fate for organic chemicals, CRC Press, 2006.

[45] A.I. Calvo, V. Pont, C. Liousse, B. Dupre, A. Mariscal, C. Zouiten, E. Gardrat, P. Castera, C.G. Lacaux, A. Castro, R. Fraile, Chemical composition of urban aerosols in Toulouse, France during CAPITOUL experiment, Meteorol. Atmos. Phys. 102 (2008) 307–323.

[46] M. Huang, Z. Wang, L. Hao, W. Zhang, Density functional theory study on the mechanism of OH-initiated atmospheric photooxidation of ethylbenzene, J. Mol. Struct. 944 (2010) 21–33.

[47] I.V. Tokmakov, G.-S. Kim, V.V. Kislov, A.M. Mebel, M.C. Lin, The reaction of phenyl radical with molecular oxygen: a G2M study of the potential energy surface, J. Phys. Chem. A 109 (2005) 6114–6127.